American Mineralogist, Volume 78, pages 724–732, 1993

Spin glass behavior in a single crystal of chromite

Kevin Severance, Ronald Edge
Department of Physics and Astronomy, University of South Carolina, Columbia, South Carolina 29208, U.S.A.
W. E. Sharp
Department of Geological Sciences, University of South Carolina, Columbia, South Carolina 29208, U.S.A.

Abstract

Elastic neutron scattering experiments on a single crystal of chromite $(Fe_{0.38}Mg_{0.62})_{1.02}$-$(Cr_{0.62}Al_{0.38})_{1.98}O_4$ from room temperature down to 2.4 K showed no crystallographic transition (cubic to tetragonal), in contrast to previous studies on synthetic polycrystalline iron chromite and synthetic magnesium chromite. Although no long-range magnetic order was observed down to 2.4 K, there was a diffuse peak showing short-range magnetic order (with a correlation length, ξ, ranging from ~10 to ~18 Å between 2.4 and 45 K), which vanished at ~50 K. The propagation vector, τ, parallel to [110] had a magnitude of ~0.106 $Å^{-1}$. Results of ac and dc susceptibility experiments indicated spin glass behavior as shown by irreversibility in the low-temperature magnetization and a sharp cusp in the susceptibility, whose maximum corresponded to a freezing temperature $T_f \sim 32.3$ K. Increasing the frequency of the ac driving field from 100 Hz to 1 kHz at low temperatures caused an upward shift in the maximum susceptibility temperature by 2 K. A modified magnetic phase diagram for the normal spinel system is presented.

Spinel structure

On account of the large number of representatives that crystallize with a spinel structure and their inclination to form extensive solid solution series, spinels are the best known ternary compounds besides perovskites. The spinels usually have the formula AB_2X_4, where A is a divalent cation, B is a trivalent cation, and X is a divalent anion. The face-centered cubic spinel structure, shown in Figure 1a, has a large unit cell ($a \sim 8$ Å). Metal ions are located in interstitial positions of a cubic closest-packed array of anions. The two types of available interstices are referred to as the tetrahedral or A sites and the octahedral or B sites. Of the 64 interstices coordinated by four O^{2-} ions in the closest packing, eight tetrahedral interstices are occupied. Sixteen of the 32 interstices coordinated by six O^{2-} ions are occupied. When the A sites are occupied by divalent cations and the B sites are occupied by trivalent cations, the structure is referred to as a normal spinel. When the A sites are occupied by trivalent cations and the B sites are occupied by a random arrangement of divalent and trivalent cations, the structure is referred to as an inverse spinel. An intermediate arrangement called mixed spinel structure is also possible.

A number of effects determine the distribution of the metal ions between the tetrahedral and octahedral sites. Since the A sites are smaller than the B sites, smaller ions, which typically have a higher charge, tend to occupy the tetrahedral sites. However, the Madelung energy becomes more favorable when trivalent cations occupy the octahedral sites, where they are coordinated by a large number of anions. Also, some cations prefer certain sites on account of their electronic configurations. For example, Zn^{2+} and Ga^{3+} ions with a d^{10} configuration form partially covalent bonds in the tetrahedral interstices, and the energy of ions with a d^3 (Cr^{3+}) or a d^8 (Ni^{2+}) configuration in octahedral interstices is substantially lowered by crystal field effects (Calhoun, 1970). Since so many effects are involved, the site occupancy of any cation generally is determined by the other cations present in the spinel.

Chromite is one of the commonest representative subgroups of spinels with the formula AB_2X_4, among which are eight oxides, seven sulfides, four selenides, one telluride, and over 100 series of solid solutions. Because of the strong preference of Cr^{3+} for octahedral sites, simple chromite has a normal spinel structure. The substitution of other cations for Cr in a solid solution series is quite extensive so long as the following criteria are fulfilled: atoms replacing each other must be of similar size (ionic or metallic radii), have the same average charge or charge compensation by coupled substitution, and have a similar mechanism of chemical bonding.

Discussion of modified phase diagram

Poole and Farach (1982) developed a qualitative magnetic phase diagram for the spinel group in terms of their respective magnetic cation concentrations in both the tetrahedral (C_A) and octahedral sites (C_B). The single-crystal chromite in this study is the first chromite sample in the composition range that does not fall on the edge of the phase diagram and is the first sample to provide experimental evidence that is consistent with the spin glass re-

0003–004X/93/0708–0724$02.00

gion in the magnetic phase diagram of Poole and Farach. The neutron scattering study and susceptibility measurements of this work provide the first evidence of spin glass behavior in chromite. No previous study has conclusively shown spin glass behavior of chromite.

A spin glass is a collection of magnetic dipole moments in a frozen disordered state. The orientations of the magnetic dipole moments in a spin glass are spatially random, as in a paramagnet, but unlike a paramagnet the orientations are retained for a long period of time. In order to produce such a state with random spatial spin orientations, the interactions must exhibit some randomness. In canonical spin glasses—dilute alloys of transition metals in noble metal hosts—the randomness occurs because the number of the magnetic atoms in the host is below the percolation limit (i.e., the interactions are not continuous throughout the entire medium). The exchange interaction of the spin with its neighbors can change sign with distance, favoring either parallel or antiparallel alignment of spins. Because the distances between the spins in a spin glass are random, a given spin is subject to interactions of both signs (+ for ferromagnetic, − for antiferromagnetic). In general, no particular spin alignment is favored and the spins are said to be frustrated.

We can cite several experimental phenomena characterizing the spin glass state below T_f, such as a frozen in magnetic moment, μ; a lack of long range spatial order; and magnetic relaxation on long time scales upon changing the applied magnetic field. Although the average magnetization vanishes in a spin glass, as in the case of a paramagnet, the local spontaneous magnetization is nonzero at a given structure site. The cusp in the curve of susceptibility vs. temperature of a spin glass suggests a second-order phase transition between the paramagnetic state (disordered in both space and time) and the spin glass state, characterized by nonvanishing permanent local spontaneous magnetizations.

According to Moorjani and Coey (1984), these canonical spin glasses have the following characteristic magnetic properties. At the freezing temperature T_f a sharp cusp appears in the low-field (<10 Oe) ac susceptibility, the temperature of which increases with increasing frequency. This peak becomes further broadened in ac or dc fields of only a few hundred Oersteds. The susceptibility of the spin glass is roughly $1/10$ that of the ferromagnet. The magnetization of the sample cooled in the absence of an applied magnetic field (zfc) depends on its thermal history. Irreversible behavior dependent on a hysteresis effect occurs near T_f, where there is a sudden loss of rotational freedom when the magnetic dipole moments become frozen. There is a discontinuity at T_f of the temperature derivative of the magnetization measured in small fields. The remanence (i.e., the field remaining after the applied field approaches zero) decays linearly wth time, t, proportional to ln t, or proportional to $t^{-1/n}$ where $n \sim 10$. The paramagnetic Curie temperature may be extrapolated from susceptibility data well above T_f and proves to be finite, close to zero, and either positive or negative.

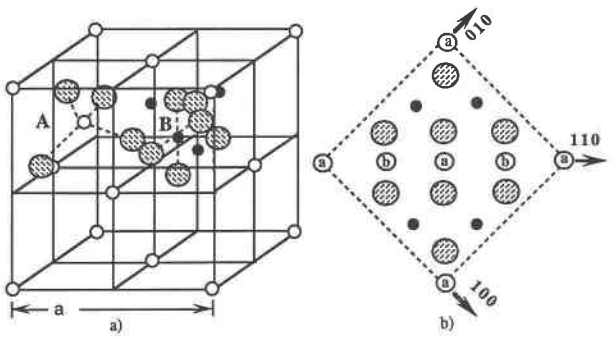

Fig. 1. (a) Unit cell of spinel in which the atoms are shown for two octants. The large shaded spheres represent O ions, the small black spheres are ions in the octahedral (B) sites, and the small white spheres are ions in the tetrahedral (A) sites. (b) Projection of atoms onto the (100) face of the unit cell. The small white spheres represent A sites 1/8 above (a) or 1/8 below (b) the plane of the figure. The face-centered array of O atoms is shown by the large shaded circles.

Many magnetic properties, such as T_f and the magnitude of the remanence, vary with the concentration of the dilute magnetic impurities. The magnetic specific heat exhibits a broad maximum at temperatures exceeding T_f by ~20%, and its peak becomes progressively broadened with increasing applied magnetic field. For $T < T_f$ the magnetic specific heat varies approximately linearly with the temperature. Such characteristics in a material are strong evidence for spin glass behavior.

Very few reports of spin glass behavior in minerals exist, and they all are from silicates. Ballet et al. (1985) observed spin glass behavior in the phyllosilicate minnesotaite. This was based on the irreversibility of low-field susceptibility measurements at low temperatures when cooled in the presence and absence of an applied magnetic field. But the neutron diffraction and Mössbauer spectroscopy studies of Townsend et al. (1985) showed that the overall magnetic structure of minnesotaite is antiferromagnetic. The spin glass behavior in the tetragonal A_2X_3-type oxide, braunite, was established by the neutron diffraction experiments of Wurmbach et al. (1981) and the susceptibility measurements of Westerholt et al. (1986).

Poole and Farach (1982) proposed a qualitative magnetic phase diagram for the normal spinel system based on exchange interactions between nearest neighbor cations of various types. Spinels with magnetically occupied A sites and nonmagnetically occupied B sites, as well as spinels with magnetically occupied B sites and nonmagnetically occupied A sites, tend to order antiferromagnetically due to negative exchange interactions. Spinels in which both the A and B sites are magnetically occupied tend to order ferrimagnetically. Spin glass ordering can occur along the C_B axis but not along the C_A axis, because the B site is frustrated, although the A site is not. This is why the spin glass region of the phase diagram intersects the C_B axis and not the C_A axis.

Unfortunately, the only experimental evidence cited by

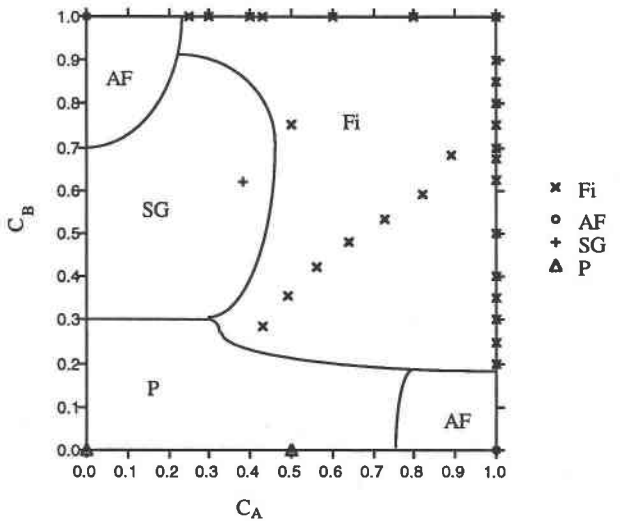

Fig. 2. Modified magnetic phase diagram for normal spinels showing the position of the single-crystal chromite in the spin glass region. C_A and C_B are the respective magnetic cation concentrations of the A and the B sites. P = paramagnetic; AF = antiferromagnetic; Fi = ferrimagnetic; and SG = spin glass. The ferrimagnets in the nonborder region are not chromite.

Poole and Farach (1982) that supported their phase diagram was spinels whose compositions lie on three of the four corners. A more thorough literature search and new evidence provided by the experiments of this work have made possible an improved modification of the magnetic phase diagram for the normal spinel system, shown in Figure 2. The magnetic orderings cited in Table 1 refer to the ground state of the spinels at low temperatures. Although the cations of the Ti-substituted system (Schindler et al., 1970) cited in Table 1 have mixed structure, these ferrimagnets have been included in Figure 2 because of the lack of data for spinels whose compositions do not lie along the border of the phase diagram.

Because the spin glass region for natural chromite is determined by the proper combination of Mg^{2+} substituting for Fe^{2+} in the A sites and Al^{3+} substituting for Cr^{3+} in the B sites, there should be specific and limited natural conditions under which such crystallization takes place. Consequently, spin glass behavior in chromite could in the future prove to be a diagnostic tool for the recognition of specific geological environments, such as distinguishing among mantle chromite from differing sources.

Helimagnetism in chromite

Kaplan et al. (1961) investigated the ground state of tetragonally distorted spinels in the region of exchange parameter space defined by nearest neighbor *AB* and *BB* interactions. They described the ground state of these spinels in terms of an antiferromagnetic spiral that had an appreciably lower energy than that predicted by the Yafet-Kittel model (Menyuk et al., 1962; Kaplan, 1960). Upon passing from one atom to the next along the crystallographic direction in which the spiral develops, the direction of the atomic magnetic moment rotates by a small fixed angle, leading to a modulation of the periodicity, with the long period of the spiral superimposed onto the crystal lattice parameter (Kaplan et al., 1961). Results of a neutron diffraction experiment of Hastings and Corliss (1962) on the normal spinel $MnCr_2O_4$ were in good qualitative accord with the model of Kaplan et al. (1961). The neutron scattering experiments of Shirane et al. (1964) and Bacchella and Pinot (1964) on powdered samples of $FeCr_2O_4$ and a neutron diffraction study on polycrystalline $MgCr_2O_4$ by Plumier (1967) have further substantiated the validity of the spiral model.

In these neutron diffraction studies of synthetic iron chromite and synthetic magnesium chromite, a splitting of the nuclear peaks implied that the polycrystalline samples had undergone a crystallographic distortion from cubic to tetragonal ($c/a < 1$) around 135 and 10.7 K, respectively. Several satellite peaks on the flank of the normal Bragg reflection were observed and were interpreted as an incommensurate modulation of the periodicity. Both the synthetic iron chromite and the synthetic magnesium chromite showed long-range magnetic order.

Neutron diffraction

The idea of the present neutron scattering experiment on the mixed chromite was to improve the signal to noise ratio by using a single crystal and to compare our data with the results of previous neutron diffraction experiments. Specific objectives of the neutron diffraction study were as follows: (1) to observe the cubic to tetragonal crystallographic distortion, should it occur, and then measure the ratio c/a; (2) to locate short-range magnetic peaks incommensurate with the periodicity of the structure, and, if they occur, determine the direction and magnitude of the propagation vector τ; (3) to determine the nature of the magnetic ordering of the sample (i.e., ferromagnetic, antiferromagnetic, paramagnetic, or spin glass).

The sample used in this experiment was a chromite octahedron found near Hangha, Sierra Leone (Smithsonian Institution, catalogue no. 139963). This crystal, which is one of the largest chromite octahedra in the world, has the largest dimension, ~18.8 mm (mass = 6.64 g and the measured density is 4.51 g/cm³). A Cu$K\alpha$ X-ray powder diffraction pattern was used to determine the lattice parameter at room temperature to be 8.266 ± 0.001 Å. Its approximate composition of $(Mg_{1-x}Fe_x)(Cr_{1-x}Al_x)_2O_4$, where $x = 0.38$, was determined by electron microprobe analysis. More exactly, the composition determined from analysis carried out on a polished surface of a separated octahedron vertex was $(Mg_{0.619}Fe^{2+}_{0.376}Mn_{0.005})(Cr_{0.601}Al_{0.377}Fe^{3+}_{0.022})_2O_4$. Furthermore, zoning is common in minerals, and this composition may not be uniform throughout the chromite octahedron. This experiment is the first to study single-crystal chromite in this composition range by neutron diffraction. Since its composition of mixed Fe and Mg is an intermediate composition of chromite samples studied by Shirane et al. (1964) and Plumier (1967), with some Al substituting for Cr in the octahedral sites, a cubic to tetragonal crystallographic transition was an-

TABLE 1. Magnetic cation distribution of some normal spinel oxides and their respective types of magnetic ordering

Composition	C_A	C_B	Order	T_{order} (K)	Reference
$Fe_{0.38}Mg_{0.62}(Cr_{0.62}Al_{0.38})_2O_4$	0.38	0.62	SG	$T_f \sim 32.3$	this study
$MgAl_2O_4$	0	0	P		von Waldner, 1962; Stahl-Brada and Low, 1959.
$ZnAl_2O_4$	0	0	P		Schindler et al., 1970; Miyadai and Okada, 1970.
$Mg_{0.5}Ni_{0.5}Al_2O_4$	0.5	0	P		Tellier and Lensen, 1966; Lotgering, 1962.
$MgCr_2O_4$	0	1	AF	$T_N = 15$	Plumier, 1968.
$ZnCr_2O_4$	0	1	AF	$T_N = 15$	Kino and Lüthi, 1971; McGuire et al., 1952.
$CoAl_2O_4$	1	0	AF	$T_N = 4$	Greenwald et al., 1954.
$FeAl_2O_4$	1	0	AF	$T_N = 9.5$	Lotgering, 1962.
$MnCr_2O_4$	1	1	Fi	$T_c = 43$	Dwight et al., 1966; Hastings and Corliss, 1962; Edwards, 1959.
$FeCr_2O_4$	1	1	Fi	$T_c = 82$	Bacchella and Pinot, 1964; Shirane et al., 1964.
$CoCr_2O_4$	1	1	Fi	$T_c = 97$	Menyuk et al., 1964; Plumier, 1967; McGuire et al., 1952.
$CuCr_2O_4$	1	1	Fi	$T_c = 135$	Prince, 1957.
$Mn_{0.6}Li_{0.4}Fe_2O_4$	0.6	1	Fi	$T_c \sim 648$	McGuire and Ferebee, 1963.
$Cu_{0.3}Zn_{0.7}Fe_2O_4$	0.3	1	Fi	$T_c = 353$	Smolenskij, 1951.
$(Ni_{0.4}Zn_{0.575}Co^{2+}_{0.03})(Co^{3+}Fe^{3+}_{1.985})O_4$	0.43	0.998	Fi	$T_c = 465$	Marais et al., 1975.
$(Mg_{0.11}Mn_{0.1}Fe_{0.79})Mg_{0.64}Mn_{0.15}Fe_{1.21}O_4$	0.89	0.68	Fi	$T_c = 660$	Murthy et al., 1970.
$Zn_{0.6}Co_{0.5}Fe_{1.9}O_4$	0.4	1	Fi	$T_c = 379$	Rezlescu and Instrate, 1971.
$Zn_{0.75}Ni_{0.25}Fe_2O_4$	0.25	1	Fi	$T_c = 375$	Murthy et al., 1970.
$Ni_{0.975}Co_{0.025}Mn_{0.02}Fe^{3+}_{1.7}Al_{0.3}O_4$	1	0.85	Fi	$T_c = 733$	Pippin and Hogan, 1959.
$NiMn_{0.02}Fe_{0.7}Al_{1.3}O_4$	1	0.35	Fi	$T_c = 733$	Pippin and Hogan, 1959.
$NiMn_{0.02}Fe_{0.8}Al_{1.2}O_4$	1	0.4	Fi	$T_c = 353$	Pippin and Hogan, 1959.
$NiMn_{0.02}Fe_{1.25}Al_{0.75}O_4$	1	0.625	Fi	$T_c = 548$	Pippin and Hogan, 1959.
$NiMn_{0.02}Fe_{1.35}Al_{0.65}O_4$	1	0.675	Fi	$T_c = 583$	Pippin and Hogan, 1959.
$NiMn_{0.02}Fe_{1.5}Al_{0.5}O_4$	1	0.75	Fi	$T_c = 648$	Pippin and Hogan, 1959.
$NiMn_{0.02}Fe_{1.6}Al_{0.4}O_4$	1	0.8	Fi	$T_c = 693$	Pippin and Hogan, 1959.
$NiMn_{0.02}Fe_{1.8}Al_{0.2}O_4$	1	0.9	Fi	$T_c = 773$	Pippin and Hogan, 1959.
$NiFe_{1.25}Al_{0.75}O_4$	1	0.25	Fi	$T_c = 567$	Gorter, 1954.
$NiOFe_2O_3$	1	1	Fi	$T_c = 863$	Went et al., 1952.
$(NiO)_{0.8}(ZnO)_{0.2}Fe_2O_3$	0.8	1	Fi	$T_c = 763$	Went et al., 1952.
$(NiO)_{0.6}(ZnO)_{0.4}Fe_2O_3$	0.6	1	Fi	$T_c = 633$	Went et al., 1952.
$(NiO)_{0.4}(ZnO)_{0.6}Fe_2O_3$	0.4	1	Fi	$T_c = 463$	Went et al., 1952.
$(NiO)_{0.3}(ZnO)_{0.7}Fe_2O_3$	0.3	1	Fi	$T_c = 363$	Went et al., 1952.
$NiOFe_{0.5}Al_{1.5}O_3$	1	0.25	Fi	$T_c = 150$	Maxwell and Pickart, 1953.
$NiOFeAlO_3$	1	0.5	Fi	$T_c = 422$	Maxwell and Pickart, 1953.
$NiOFe_{1.5}Al_{0.5}O_3$	1	0.75	Fi	$T_c = 656$	Maxwell and Pickart, 1953.
$MnFe_{0.6}Ga_{1.4}O_4$	1	0.3	Fi	$T_c = 198$	Lensen, 1959.
$MnFeGaO_4$	1	0.5	Fi	$T_c = 331$	Lensen, 1959.
$MnFe_{1.4}Ga_{0.6}O_4$	1	0.7	Fi	$T_c = 433$	Lensen, 1959.
$MnFe_{1.6}Ga_{0.4}O_4$	1	0.8	Fi	$T_c = 473$	Lensen, 1959.
$MnFe_{1.8}Ga_{0.2}O_4$	1	0.9	Fi	$T_c = 533$	Lensen, 1959.
$Cu_{0.5}FeAl_{1.5}O_4$	1	0.25	Fi	$T_c = 296$	Lenglet, 1969.
$CoFe_{0.4}Ga_{1.6}O_4$	1	0.2	Fi	$T_c = 186$	Lensen, 1960.
$CuFeGaO_4$	1	0.5	Fi	$T_c = 409$	Lenglet and Tellier, 1968.
$CuFe_{0.6}Ga_{1.2}O_4$	1	0.4	Fi	$T_c = 310$	Obi, 1974.
$CuFe_{0.6}Ga_{1.4}O_4$	1	0.3	Fi	$T_c = 204$	Obi, 1974.
$Fe^{2+}(Fe^{3+}_{0.4}Ga_{1.6})O_4$	1	0.2	Fi	$T_c = 206$	Lensen, 1960.
$Ni_{1.5}FeTi_{0.5}O_4$	1	0.75	Fi	$T_c = 566$	Gorter, 1954.
$NiZn_{0.5}FeTi_{0.5}O_4$	0.5	0.75	Fi	$T_c = 498$	Gorter, 1954.
$(Mg_{0.18}Fe^{3+}_{0.82})(Fe^{3+}_{1.18}Mg_{0.82})O_4$	0.82	0.59	Fi	$T_c = 648$	Tellier and Lensen, 1966.
$(Mg_{0.27}Fe^{3+}_{0.73})(Fe^{3+}_{1.07}Mg_{0.83}Ti_{0.1})O_4$	0.73	0.535	Fi	$T_c = 558$	Tellier and Lensen, 1966.
$(Mg_{0.36}Fe^{3+}_{0.64})(Fe^{3+}_{0.96}Mg_{0.84}Ti_{0.2})O_4$	0.64	0.48	Fi	$T_c = 483$	Tellier and Lensen, 1966.
$(Mg_{0.44}Fe^{3+}_{0.56})(Fe^{3+}_{0.84}Mg_{0.86}Ti_{0.3})O_4$	0.56	0.42	Fi	$T_c = 407$	Tellier and Lensen, 1966.
$(Mg_{0.51}Fe^{3+}_{0.49})(Fe^{3+}_{0.71}Mg_{0.89}Ti_{0.4})O_4$	0.49	0.355	Fi	$T_c = 319$	Tellier and Lensen, 1966.
$(Mg_{0.57}Fe^{3+}_{0.43})(Fe^{3+}_{0.57}Mg_{0.93}Ti_{0.5})O_4$	0.43	0.285	Fi	$T_c = 203$	Tellier and Lensen, 1966.

Note: AF = antiferromagnetic; Fi = ferrimagnetic; P = paramagnetic; SG = spin glass.

ticipated. Hence, the sample was packed in Al foil to allow for the stress should such a transition occur, and the specimen was cooled slowly.

The elastic neutron scattering experiment was performed at the High Flux Isotope Reactor at Oak Ridge National Laboratory using neutrons with energy of 14.8 meV ($\lambda = 2.35$ Å). Neutron diffraction data were gathered from room temperature down to the minimum (10 K) of the Displex refrigerator. Then liquid He was added to the cryostat, and, by pumping to reduce the pressure, the temperature was lowered to 2.4 K. No splitting of the Bragg peaks was observed down to 2.4 K, and hence the

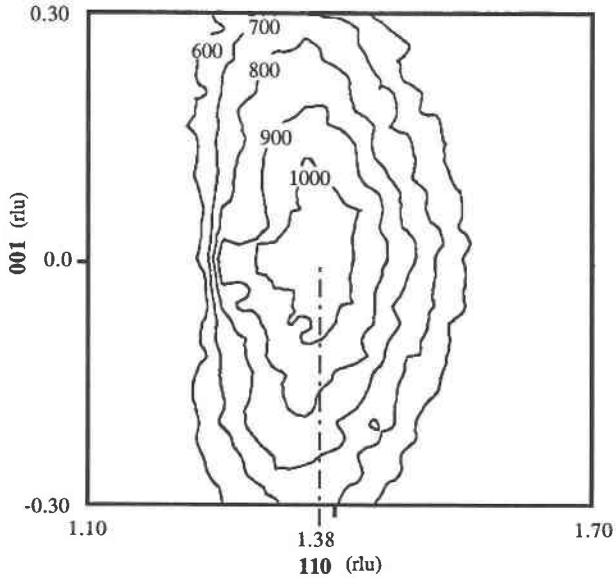

Fig. 3. The diffuse neutron magnetic peak of the Sierra Leone chromite sample at 1.38, 1.38, 0. The contours represent intensity.

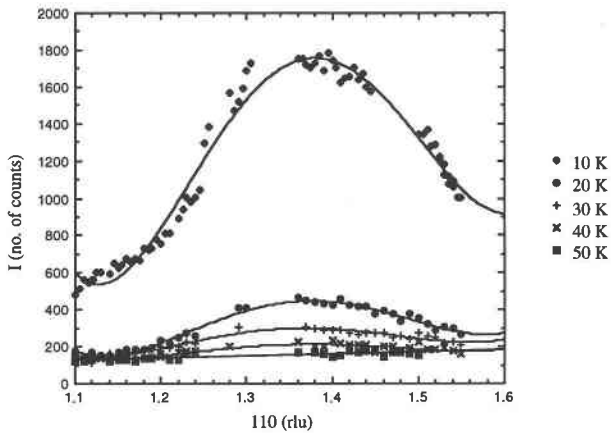

Fig. 4. The intensity of the diffuse magnetic peak as a function of temperature from 10 to 50 K along the [110] direction.

cubic to tetragonal distortion that occurs in $FeCr_2O_4$ and $MgCr_2O_4$ did not occur. An incommensurate diffuse magnetic peak was found along the [110] direction at reciprocal lattice units ~1.38, 1.38, 0 and ~2.62, 2.62, 0. A contour plot of the grid scan data shows the shape of this magnetic satellite peak at 10 K (Fig. 3), which has a correlation length of about 10 Å along [001] and about 18 Å along the [110] direction. As a result of the face-centered cubic crystal structure, the correlation length is larger along the [110] direction because the magnetic ions are closer together (see Fig. 1b) and have stronger interactions along [110].

Figure 4 shows the data of the longitudinal magnetic satellite peak at 1.38, 1.38, 0 as a function of temperature, which has been fitted to a fourth-order polynomial for data 10–40 K and to a line at 50 K. Higher order Bragg peaks corresponding to the nuclear crystal structure have been deleted, leaving only the diffuse magnetic peaks. As the temperature increased from 10 to 45 K, the intensity decreased linearly, while the full width at half maximum (FWHM) broadened from ~0.8 to ~1.2 reciprocal lattice units (rlu). The correlation length, ξ, changed from ~10 Å at 10 K to ~7 Å at 45 K. The values of the intensity and the FWHM of the diffuse magnetic peak were determined by data fitting to a Lorentzian distribution by the method of least squares. At 50 K the intensity of the diffuse peak had diminished to the background level, indicating that short-range magnetic order had completely vanished. The propagation vector, τ, for the spin system had a magnitude of ~0.106 $Å^{-1}$ parallel to the [110] direction. In contrast to the studies of polycrystalline synthetic $FeCr_2O_4$ and synthetic $MgCr_2O_4$, no long-range magnetic order was observed at 2.4 K, and the slope of the FWHM vs. temperature curve (Fig. 5) gives no indication that the sample orders above absolute zero. The other magnetic peaks that had been found in polycrystalline samples of synthetic $FeCr_2O_4$ and synthetic $MgCr_2O_4$ around the (111) and (010) Bragg reflections were not observed in the mixed chromite single crystal.

Discussion of the neutron diffraction experiment

Lyons and Kaplan (1960) have shown that the classical ground state of a tetragonally distorted spinel should be a magnetic spiral structure. This state is lower than the ground state obtained by the Yafet-Kittel model, and the Yafet-Kittel triangular configuration is never the ground state for cubic spinels (Kaplan, 1960).

According to the model of Hastings and Corliss (1962), for spins that belong to a given sublattice, the directions of the spins lie on a cone with a fixed half-angle. The axial components of spins are constant on the sublattice, and the transverse components of these same spins rotate in discrete steps under translation along the propagation direction to equivalent sites in other unit cells. Each sublattice is characterized by a particular cone angle, α, and a particular phase angle for the rotation of the transverse component. The axes of cones corresponding to different sublattices are always parallel, but they do not necessarily coincide with the direction of the propagation of the spiral. Figure 6a is a schematic illustration of a magnetic spiral. Figure 6b shows spin vector μ lying on a cone with half-angle α. The scattering vector for a given reflection is κ, whereas τ denotes the propagation vector for the transverse component of the spin system. The γth spin in the nth unit cell is given by Equation 1.

$$\mathbf{S}_{n\gamma} = |S\gamma| \sin \alpha_\gamma \left[\frac{\hat{u}_1 - i\hat{u}_2}{2} \exp(i2\pi\tau \cdot \mathbf{r}_{n\gamma}) e^{i\phi}_\gamma + \text{complex conjugate} \right] + \hat{u}_3 |S_\gamma| \cos \alpha_\gamma. \quad (1)$$

The phase angle of the γth spin in the unit cell is ϕ_γ, the

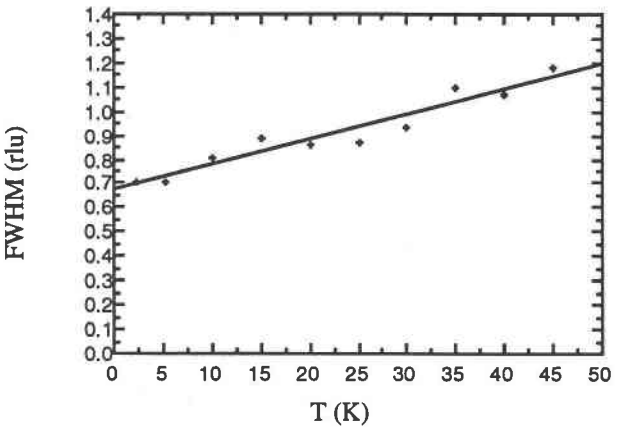

Fig. 5. The full width at half maximum (FWHM) vs. temperature curve of 1.38, 1.38, 0 transverse data. In order for long-range magnetic order to occur, the FWHM in $Å^{-1}$ must approach zero so that the correlation length may tend to infinity.

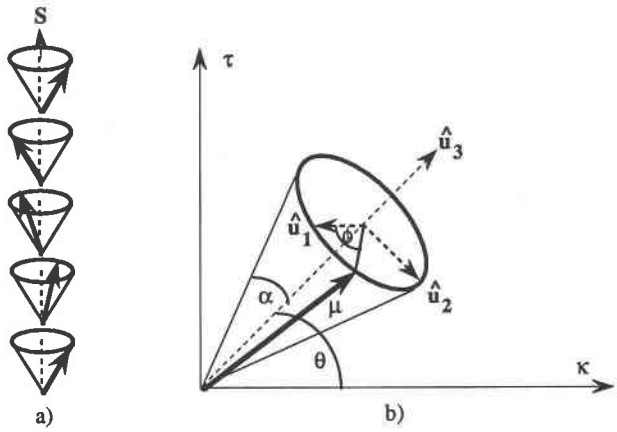

Fig. 6. (a) Magnetic spiral arrangement. (b) The spin vector μ lies on a cone of half-angle α. Note that the propagation vector τ does not coincide with the symmetry axis of the cone.

position vector is $\mathbf{r}_{m\gamma}$, and the angle between the scattering vector and the cone axis is θ.

The incommensurate satellite reflections along the flanks of the strong fundamental reflections were observed at τ away from the reciprocal lattice point {2, 2, 0}, where $\tau = \pm\delta[110]$ with $\delta = 0.62$ rlu, as shown in Figure 7. Funahashi et al. (1987) observed a similar satellite peak in the synthetic helimagnet $CoCrO_4$ at τ away from the fundamental reflections, where $\tau = \pm\delta[110]$ with $\delta = 0.63$. For the sake of clarity, to remain consistent with the expression defining the magnetic spiral structure ($e^{i2\pi\tau\cdot r}$), and for the purpose of comparing our observed magnitude of τ to the magnitudes of τ from chromite in previous studies, the explicit calculation of τ is as follows:

$$|\tau| = \left[\frac{0.62}{a}\right]\sqrt{2}$$

where the lattice parameter $a = 8.266$ Å

$$|\tau| = 0.106 \text{ Å}^{-1}. \quad (2)$$

The calculated magnitude of the propagation vector, $|\tau|$, is 0.106 $Å^{-1}$, and it lies along the [110] direction in the single-crystal chromite. This value is larger than the respective values of 0.037 and 0.063 $Å^{-1}$ observed by Bacchella and Pinot (1964) and by Shirane et al. (1964) for $FeCr_2O_4$ along the same direction. The reciprocal of $|\tau|$ is the wavelength of the modulation ($\lambda = \tau^{-1} = 9.43$ Å). The wavelength of the modulation is larger than the lattice parameter by a factor of 1.14.

A plot of the full width at half maximum (FWHM) in reciprocal lattice units vs. temperature in Kelvin is shown in Figure 5. Clearly, the slope of the line cannot intersect the **x** axis above absolute zero. This means that the sample will not order above 0 K, and that the sample is either a paramagnet or a spin glass. The elastic scattering experiment cannot distinguish a paramagnet from a spin glass. Consequently, susceptibility measurements were conducted and the results are discussed below.

Magnetic susceptibility measurements

Three types of magnetometer systems were used in this study. The magnetization as a function of applied magnetic field at 4 K was measured using a vibrating sample magnetometer (VSM) technique (Foner, 1959). We have used a standard mutual inductance technique (Hartshorn, 1925) for the ac susceptibility measurements at frequencies of 100 Hz and 1 kHz. A Magnetic Property Measurement System superconducting quantum-interference device (SQUID) magnetometer was used for the magnetization measurements in very low fields. All of these measurements were made on the equipment of the Solid State Division at Oak Ridge National Laboratory.

The purpose of the susceptibility experiments was to differentiate between spin glass and paramagnetic behavior. If the sample were a paramagnet, the plot of the susceptibility vs. temperature would not show a peak or cusp and the plot of the inverse susceptibility as a function of temperature would be linear (Kittel, 1986). One characteristic of spin glass behavior (Moorjani and Coey, 1984) is the junction in the susceptibility vs. temperature curves when the sample is field cooled (fc) compared with when it is cooled in the absence of a magnetic field (zfc). All of the susceptibility measurements in this work were made along the [111] direction. Notice that in Figure 8 the plot of the magnetization as a function of temperature has the same shape as the susceptibility curve (Fig. 9) and exhibits two curves of characteristically different shapes, corresponding to fc and zfc. The deviation in fc and zfc magnetization curves marks the onset of relaxation processes. The temperature corresponding to the maximum of the curve in Figure 8 at about 30 K is called the freezing temperature, T_f, the temperature below which the magnetic dipole moments of the material are locked into their random positions. This temperature, approximately 30 K, is slightly lower than the freezing temperatures defined by the susceptibility maxima in the ac susceptibility measurements. The maximum of the magnetization

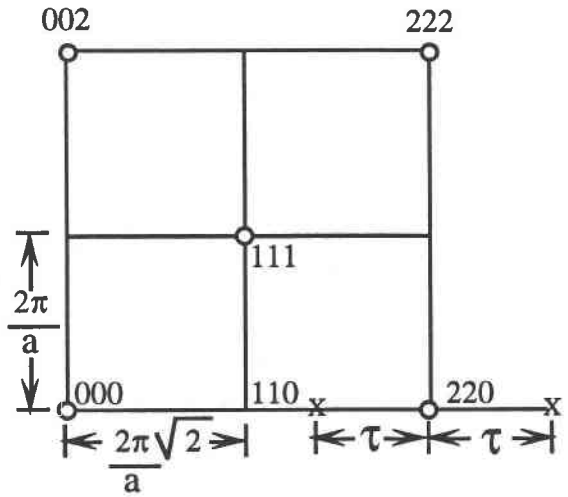

Fig. 7. Location of the satellite peak in reciprocal lattice space. The satellite peaks are indicated with an X at a distance $\pm\tau$ away from the fundamental reflection at (220). The small circles represent fundamental reflections.

cooled in an applied magnetic field of 100 Oe corresponds to a magnetic moment of $\sim 2 \times 10^{-5}$ μ_B pfu.

Irreversibility of the magnetization as a function of the applied external magnetic field is also a common phenomenon in spin glasses that does not occur in ferri- or ferromagnets. Figure 10 shows a plot of M vs. H at 4 K. The deviation in the magnetization upon completion of the hysteresis loop or remanence is ~0.2 Oe. Such remanent magnetization is consistent with the expected behavior of a spin glass.

Another important characteristic of a spin glass is the shift in T_f toward a higher temperature with an increase in the frequency in the ac driving field during susceptibility measurements (Moorjani and Coey, 1984). Plots of χ (ν) as a function of temperature at frequencies of ~100 Hz and ~1 kHz are shown in Figure 9. The upper curve shows ac susceptibility as a function of temperature at a frequency of 100 Hz. The lower plot shows ac susceptibility as a function of temperature at a frequency of 1 kHz. Both of the ac susceptibility maxima were determined by fits to a fourth-order polynomial. Notice that increasing the driving frequency of the ac driving field from 100 Hz to 1 kHz shifts the maxima in the susceptibility from ~32.3 to ~34.3 K.

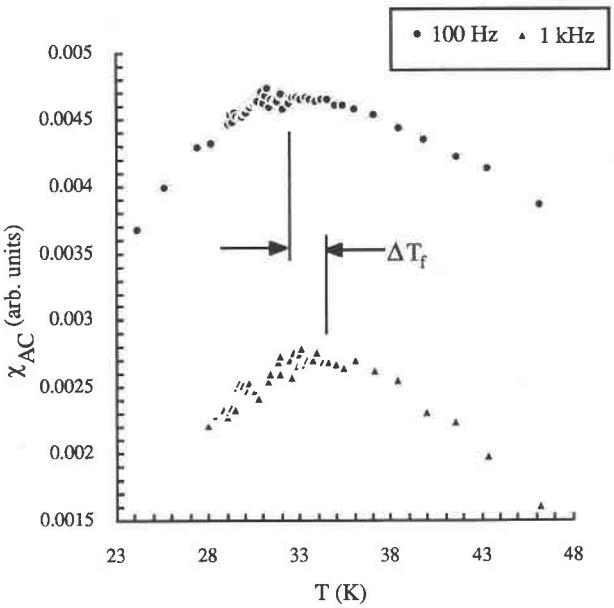

Fig. 9. Shift in the freezing temperature from T_f = 32.3 K (ν = 100 Hz) to T_f = 34.3 K (ν = 1 kHz).

Westerholt et al. (1986) observed that ac driving fields between 0.1 and 10 Oe had no noticeable effect on χ_{ac} in their study of braunite. So a constant ac field of about 3.5 Oe was used throughout these measurements, with the

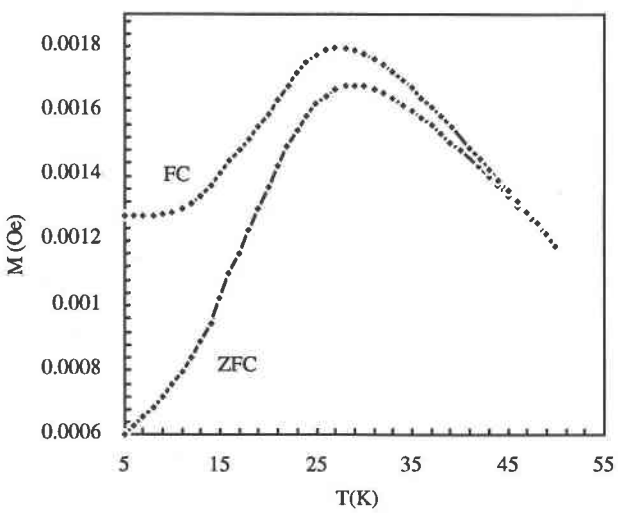

Fig. 8. The magnetic moment as a function of temperature after cooling in a 100-Oe applied magnetic field (FC) and after cooling in the absence of an applied magnetic field (ZFC).

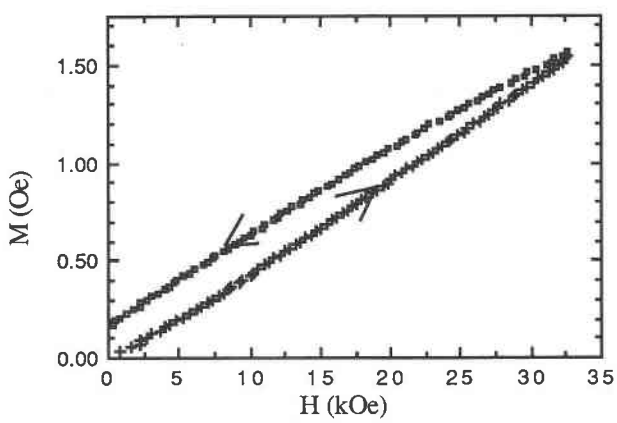

Fig. 10. Irreversibility in the magnetic behavior of the Sierra Leone chromite sample at 4 K.

mutual inductance bridge apparatus previously described. The freezing temperature, T_f, of the ac susceptibility curve shifted upward by approximately 2 K when the frequency was increased by one order of magnitude. This corresponds to

$$\frac{\Delta T_f}{T_f(\Delta \log_{10} \nu)} = 0.077.$$

Conclusions

The anticipated cubic to tetragonal crystallographic distortion observed in other polycrystalline synthetic chromite never occurred for the single-crystal chromite of mixed cation composition. A diffuse peak showing short-range magnetic order was observed on the flanks of an atomic Bragg peak. The periodicity of this magnetic peak is incommensurate with that of the lattice sites, and the wavelength of the modulation is larger than the lattice parameter by a factor of 1.14. The magnitude of the propagation vector τ is ~ 0.105 Å^{-1}, and τ is parallel to the [110] direction. The correlation length of this short-range magnetic order ranged from ~ 10 to ~ 18 Å in the temperature range of 2.4–45 K and vanished at ~ 50 K.

The lack of long-range magnetic order as determined by neutron diffraction eliminated the possibility that the sample was an antiferromagnet, implying that the chromite was either a paramagnet or a spin glass. The sharp cusp in the dc susceptibility as a function of temperature curve ruled out the possibility of paramagnetism. Furthermore, the irreversibility in the magnetization, along with the frequency dependence of the ac susceptibility, support the occurrence of spin glass behavior in the single-crystal chromite from Sierra Leone.

Acknowledgments

We are grateful to the Southeastern Universities Research Association (SURA) for supporting this project with a grant and to the Smithsonian Institution for the loan of the chromite specimen (catalogue no. 139963). We thank the Solid State Division at Oak Ridge National Laboratory (ORNL) for the use of the equipment, Joe Cable of the Solid State Division at ORNL for his collaboration in the neutron diffraction experiment, H.R. Kerchner of ORNL, G. Ossandan, and Y.R. Sun of the University of Tennessee, Knoxville, for their help with the susceptibility measurements, and John Shervais from the Department of Geological Sciences at the University of South Carolina for determining the chemical composition.

References cited

Bacchella, G., and Pinot, M. (1964) Etude sur la structure magnètique de $FeCr_2O_4$. Journal de Physique et de Radium, 25, 537–541.

Ballet, O., Coey, J., Mangin, P., and Townsend, M. (1985) Ferrous talc: A planar antiferromagnet. Solid State Communications, 11, 787–790.

Calhoun, B. (1970) Landolt-Börnstein neue Serie, Gruppe 3, Band 4, Teil b, p. 51–64. Springer-Verlag, Berlin.

Dwight, K., Menyuk, N., Feinlieb, J., and Wold, A. (1966) Reduced manganese moment in manganese chromite. Journal of Applied Physics, 33, 962–964.

Edwards, P. (1959) Magnetic properties of the manganese chromite-aluminates. Physical Review, 116, 294–300.

Foner, S. (1959) Versatile and sensitive vibrating-sample magnetometer. Reviews of Scientific Instruments, 30, 548–557.

Funahashi, S., Morii, Y., and Child, H. (1987) Two-dimensional observation of neutron diffraction of $CoCr_2O_4$ with wide angle neutron diffractometer WAND. Journal of Applied Physics, 61, 4114–4116.

Gorter, E. (1954) Saturation magnetization and crystal chemistry of ferrimagnetic oxides. Philips Research Reports, 9, 295–443.

Greenwald, S., Pickart, S., and Grannis, F. (1954) Cation distribution and g factors of certain spinels containing Ni^{++}, Mn^{++}, Co^{++}, Al^{+++}, Ga^{+++}, and Fe^{+++}. Journal of Chemical Physics, 22, 1597–1600.

Hartshorn, L. (1925) Comparison of mutual inductances at telephonic frequencies. Journal of Scientific Instruments (GB), 2, 145–151.

Hastings, J., and Corliss, L. (1962) Magnetic structure of manganese chromite. Physical Review, 126, 556–565.

Kaplan, T. (1960) Classical theory of spin configurations in the cubic spinel. Physical Review, 119, 1460–1470.

Kaplan, T., Dwight, K., Lyons, D., and Menyuk, N. (1961) Classical theory of the ground spin state in spinels. Journal of Applied Physics, 32, 13S–20S.

Kino, Y., and Lüthi, B. (1971) Magnetic and elastic properties of zinc-chromite. Solid State Communications, 9, 805–808.

Kittel, C. (1986) Introduction to solid state physics (6th edition), 396 p. Wiley, New York.

Lenglet, M. (1969) The $CuFe_2O_4$-$CuAl_2O_4$ system. Revue de Chimie Minérale, 6, 703.

Lenglet, M., and Tellier, J. (1968) Etude du systeme $CuFe_2O_4$-$CuGa_2O_4$. Comptes Rendus Hebdomadaires des Séances de l'Academie des Sciences Series C, 267, 525–527.

Lensen, M. (1959) Substitution in some spinel ferrites of the ferric ion by trivalent vanadium and gallium ions. Annales de Chimie (Paris), 4, 891–947.

——— (1960) Structural studies of the gallates of manganese, iron, and cobalt. Annales de Chimie (Rome), 4, 891.

Lotgering, F. (1962) Paramagnetic susceptibilities of Fe^{2+} and Ni^{2+} ions at tetrahedral or octahedral sites of oxides. Journal of the Physics and Chemistry of Solids, 23, 1153–1167.

Lyons, D., and Kaplan, T. (1960) Method for determining the ground-state spin configurations. Physical Review, 120, 1580–1585.

Marais, A., Merceron, T., and Porte, M. (1975) Effect of tetragonal distortion on the directional order in copper ferrite at high temperature. American Institute of Physics Conference Proceedings, 29, 558.

Maxwell, L., and Pickart, S. (1953) Magnetization in nickel ferrite-aluminates and nickel ferrite-gallates. Physical Review, 92, 1120–1126.

McGuire, T., and Ferebee, F. (1963) Magnetic properties of lithium-substituted manganese ferrite. Journal of Applied Physics, 34, 1821–1823.

McGuire, T., Howard, L., and Smart, J. (1952) Magnetic properties of the chromites. Ceramic Age, 60, 22–24.

Menyuk, N., Dwight, K., Lyons, D., and Kaplan, T. (1962) Classical theory of the ground spin-state in normal tetragonal spinels. I. Neel, Yafet-Kittel, and collinear antiferromagnetic modes. Physical Review, 127, 1983–1996.

Menyuk, N., Dwight, K., and Wold, A. (1964) Ferrimagnetic spiral configurations in cobalt chromite. Journal de Physique et de Radium, 25, 528–536.

Miyadai, T., and Okada, T. (1970) On the angular dependence of line width of ESR for Cr^{+3} in $ZnAl_2O_4$ single crystal. Journal of the Physical Society of Japan, 29, 1108–1109.

Moorjani, K., and Coey, J. (1984) Magnetic glasses, p. 36–37. Elsevier, Amsterdam.

Murthy, N., Natera, M., Begum, R., and Youssef, S. (1970) Magnetic structures of some spinel ferrites determined by polarized and unpolarized neutron diffraction. Proceedings of the International Conference on Ferrites, Kyoto, Japan, July 1970, 60–63.

Obi, Y. (1974) On the crystal distortion in several spinel systems. Physica Status Solidi (a), 25, 293–299.

Pippin, J., and Hogan, C. (1959) Scientific report no. 1: Resonance measurements on Ni-Co ferrites as a function of temperature and on Ni ferrite-aluminates. Gordon McKay Lab of Applied Science, Harvard University.

Plumier, R. (1967) Etude magnétique par diffraction des neutrons du composé spinelle $MnCr_2O_4$. Comptes Rendus Hebdomadaires des Séances de l'Academie des Sciences Series B, 265, 726–729.

——— (1968) Etude par diffraction des neutrons du composé spinelle nor-

mal $MgCr_2O_4$. Comptes Rendus Hebdomadaires des Séances de l'Academie des Sciences Series B, 267, 98–101.

Poole, C., Jr., and Farach, H. (1982) Magnetic phase diagram of spinel spin-glasses. Zeitschrift für Physik B, Condensed Matter, 47, 55–57.

Prince, E. (1957) Crystal and magnetic structure of copper chromite. Acta Crystallographica, 10, 554–556.

Rezlescu, N., and Instrate, S. (1971) Cation distribution and the Curie point in Co-Zn ferrites. Revue Roumaine de Physique, 16, 591–592.

Schindler, P., Gerber, P., and Waldner, F. (1970) Electron spin resonance of Cr^{3+} in $ZnAl_2O_4$ spinel parameters and linewidths. Helvetica Physica Acta, 43, 583–592.

Shirane, G., Cox, D., and Pickart, S. (1964) Magnetic structures in $FeCr_2S_4$ and $FeCr_2O_4$. Journal of Applied Physics, 35, 954–955.

Smolenskij, G. (1951) Curie temperatures and saturation magnetizations of binary solutions of Ni-, Cu-, Mn-, and Mg ferrites. Døklady Akademie Nauk SSSR, 78, 921.

Stahl-Brada, R., and Low, W. (1959) Paramagnetic resonance spectra of chromium and manganese in the spinel structure. Physical Review, 116, 561–564.

Tellier, J., and Lensen, M. (1966) Etude de la substitution dans le ferrite de magnesium des ions ferriques par des ions tetravalents. I. Ti^{4+}. Bulletin de la Société Chimique de France, 8, 2502–2505.

Townsend, M., Longworth, G., and Roudaut, E. (1985) Field induced ferromagnetism in minnesotaite. Physics and Chemistry of Minerals, 12, 9–12.

von Waldner, F. (1962) Mn^{2+} Spektrum paramagnetischer Elektronenresonanz (EPR) in einem natürlichen $MgAl_2O_4$ Spinell. Helvetica Physica Acta, 21, 756–764.

Went, J., Rathenau, G., Gorter, E., and van Oosterhout, G. (1952) Ferroxdure, a class of new permanent magnet materials. Philips Technical Reviews, 13, 185–208.

Westerholt, K., Würmbach, I., and Dahlbeck, R. (1986) Antiferromagnetism and spin-glass order in Fe-, Ca-, and Al-substituted braunites $Mn^{2+}(Mn^{3+})_6SiO_{12}$. Physical Review B, 34, 6437–6447.

Wurmbach, I., Hewat, A., and Sabine, T. (1981) Magnetische- und Neutronenbeugungs-Experimente an Braunit, $Mn^{2+}Mn^{3+}O_8/SiO_4$. Zeitschrift für Kristallographie und Mineralogie, 154, 240–242.

Manuscript received July 22, 1992
Manuscript accepted March 16, 1993